Contrasting internally and externally generated Atlantic Multidecadal Variability and the role for AMOC in CMIP6 historical simulations

Article

Supplemental Material

Robson, J. ORCID: https://orcid.org/0000-0002-3467-018X, Sutton, R. ORCID: https://orcid.org/0000-0001-8345-8583, Menary, M. B. and Lai, M. W.K. (2023) Contrasting internally and externally generated Atlantic Multidecadal Variability and the role for AMOC in CMIP6 historical simulations. Philosophical Transactions of the Royal Society A: Mathematical, Physical and Engineering Sciences, 381 (2262). 20220194. ISSN 1471-2962 doi: 10.1098/rsta.2022.0194 Available at https://centaur.reading.ac.uk/112966/

Supplementary information for 'Contrasting internally and externally generated Atlantic Multidecadal Variability in CMIP6 historical simulations'

Jon Robson, Rowan Sutton, Matthew B. Menary, Michael Lai

August 16, 2023

1 Models used

Table S1: The CMIP6 models used in this study, the number of ensemble members used, and their ASR_HD value (computed as the change over 1850–1985 - see methodology for details). Models with an ASR_HD greater than 1.5 W m^{-2} are classified as 'strong' models, and are shown in bold text. Also shown is the mean AMOC strength at 26°N, computed as the ensemble mean for each model over the time period 1850–1879.

Centre	Model	Members	ASR_HD [W m^{-2}]	AMOC at 26°N (Sv)	Data reference	Model reference
CSIRO	**ACCESS-ESM1-5**	**9**	**1.93**	**19.7**	**Ziehn et al. (2019)**	**Ziehn et al. (2020)**
BCC	BCC-CSM2-MR	3	0.60	20.8	Wu et al. (2018)	Wu et al. (2019)
NCAR	**CESM2**	**9**	**2.51**	**18.1**	**Danabasoglu (2019a)**	**Danabasoglu et al. (2020)**
NCAR	**CESM2-WACCM**	**3**	**2.74**	**17.5**	**Danabasoglu (2019b)**	**Danabasoglu et al. (2020)**
CNRM-CERFACS	CNRM-CM6-1	9	1.04	15.1	Voldoire (2018)	Voldoire et al. (2019)
NASA-GISS	**GISS-E2-1-G (p1)**	**9**	**1.67**	**23.9**	**for Space Studies (NASA/GISS)**	**Kelley et al. (2020), Miller et al. (2021)**
MOHC	**HadGEM3-GC31-LL**	**4**	**2.47**	**14.7**	**Ridley et al. (2019a)**	**Andrews et al. (2020), Kuhlbrodt et al. (2018)**
MOHC	**HadGEM3-GC31-MM**	**4**	**2.64**	**16.8**	**Ridley et al. (2019b)**	**Andrews et al. (2020)**
INM	INM-CM5-0	5	0.52	16.0	Volodin et al. (2019)	Volodin et al. (2017), Volodin and Kostrykin (2016)
IPSL	IPSL-CM6A-LR	9	0.34	10.6	Boucher et al. (2021)	Boucher et al. (2020)
MIROC	MIROC6	9	0.81	14.6	Tatebe and Watanabe (2018)	Tatebe et al. (2019)
MPI-M	MPI-ESM1-2-HR	9	0.33	19.0	Jungclaus et al. (2019)	Mauritsen et al. (2019), Stevens et al. (2013)
MPI-M	MPI-ESM1-2-LR	9	0.01	21.8	Wieners et al. (2019)	Mauritsen et al. (2019), Stevens et al. (2013)
MRI	**MRI-ESM2-0**	**5**	**2.36**	**21.2**	**Yukimoto et al. (2019)**	**YUKIMOTO et al. (2019)**
NUIST	NESM3	5	1.28	7.3	Cao and Wang (2019)	Cao et al. (2018)
NCC	**NorESM2-LM**	**3**	**2.64**	**22.2**	**Seland et al. (2019)**	**Seland et al. (2020)**
MOHC	**UKESM1-0-LL**	**14.7**	**2.94**	**13.7**	**Tang et al. (2019)**	**Sellar et al. (2019)**

2 Additional figures

Figure S1 shows the comparison of the variability of iAMV (e.g., computed as the residual to the externally-forced, ensemble mean, component), compared to the internal variability of AMV found in piControls (cAMV) for the models. Overall, we find that the iAMV method successfully isolates the magnitude of internal variability found in the piControl simulations. In particular, the standard deviation of the linearly detrended basin-mean AMV (e.g., AMV_BM), the basin-mean sea surface temperatures (SSTs, blue dots) and the Trenberth and Shea, (2006) AMV index (AMV_TS, Trenberth and Shea (2006)) all lie broadly on the 1-to-1 line, at least broadly within sampling uncertainties. This is also largely the case when using the AMV-Glob. However, we do find that the iAMV variance is substantially larger than cAMV for models which have the largest AMV variability. We interpret this as being related to the fact that the models that have the largest AMV variability also have a large projection on global-mean temperatures. Therefore, when we regress the changes in global-mean temperatures out, then we effectively suppress the AMV variability when using the AMV-Glob index. Visual inspection of the regression patterns appears to support this interpretation (not shown). This is also particularly a problem for the AMV-Glob index in the way we have applied it. For example, in the historical we computed the impact of global-mean forced changes by regressing onto the ensemble-mean time-series. However, this is not possible in the piControl, and we simply regress global SSTs onto the global-mean temperatures. Thus, in the absence of large secular trends, such a method will remove the variability associated with AMV itself. Thus, this further underlines the sensitivity of the analysis to choices made in the definition of the AMV index.

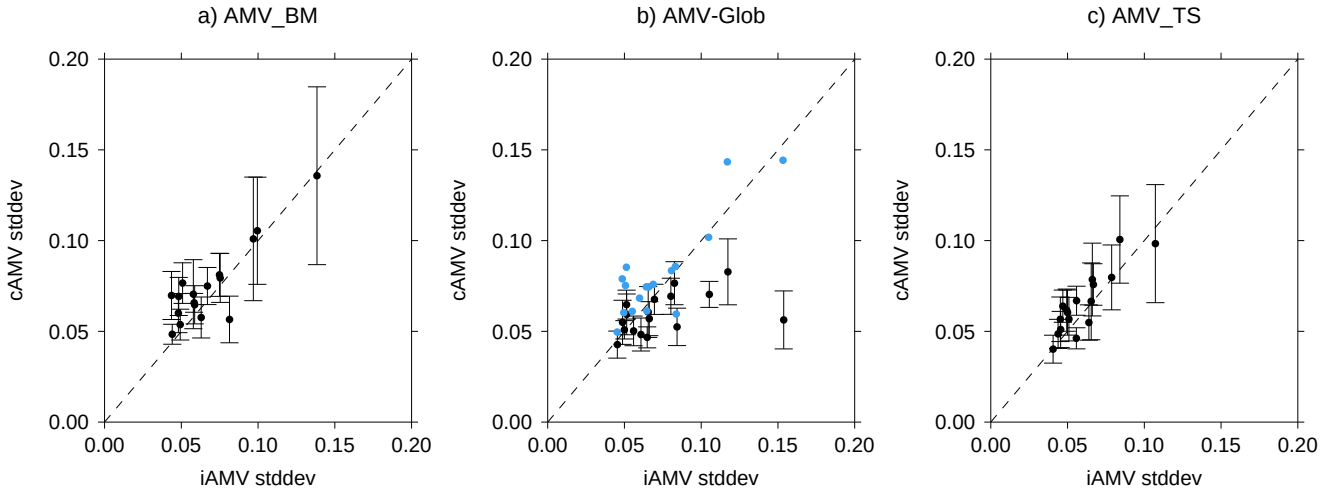

Figure S1: Shows the comparison of variance for AMV indices computed using the residual method (e.g., iAMV), and that from the piControl (cAMV), which we assume represents internal variability. a) shows the comparison for the AMV_BM index, b) for the AMV-Glob, and c) for the AMV index based on Trenberth and Shea, 2006 (AMV_TS). Black dots show the mean value of variance computed from historical or equal length chunks of the piControl. Error bars show the spread of variance computed from each member or piControl chunk individually. Blue dots on b) show the values for basin mean Atlantic temperatures, e.g., where no attempt to remove long-term signals have been attempted.

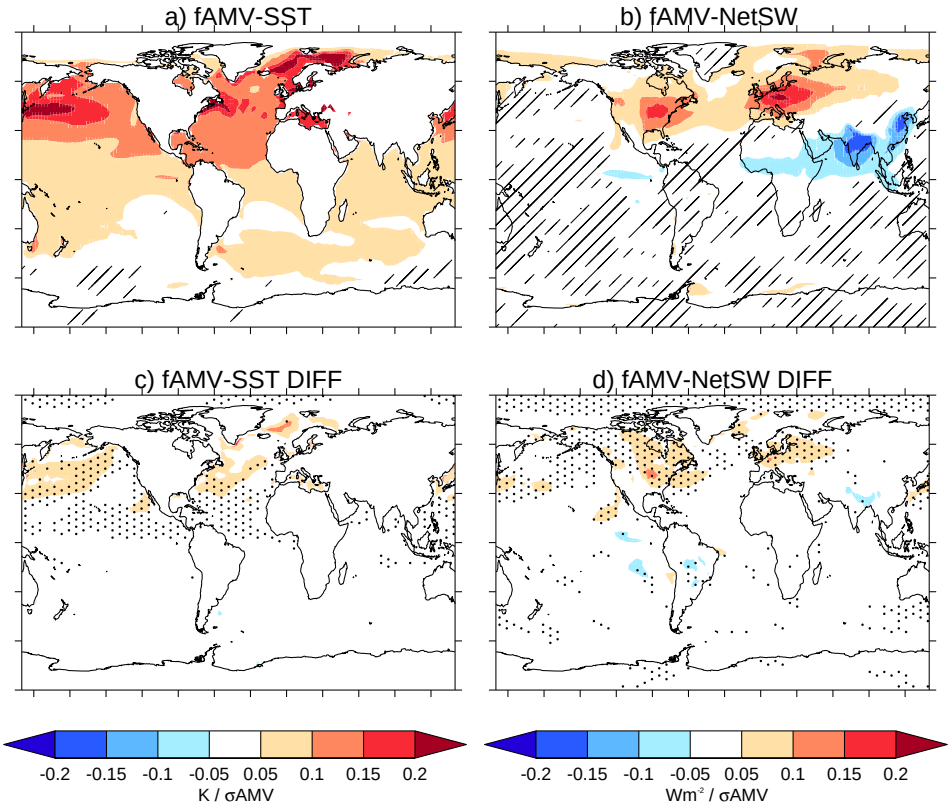

Figure S2: Shows the relationship between the fAMV_BM and surface heat fluxes. a) shows the MMM fAMV_BM SST pattern. Contours show the MMM regression pattern of SST on fAMV_BM and hatching shows where 80% of models agree on the sign of the regression slope coefficient. b) shows the same as a) but now for net surface shortwave (NetSW). c) shows the difference in the SST fAMV pattern between strong and weak models (e.g., strong *minus* weak), and stippling now shows where the difference is significant at the $p \leq 0.1$. d) shows the same as c) but for the NetSW. Note this is the same for figure 4 in the main paper, but now for AMV_BM rather than AMV-Glob.

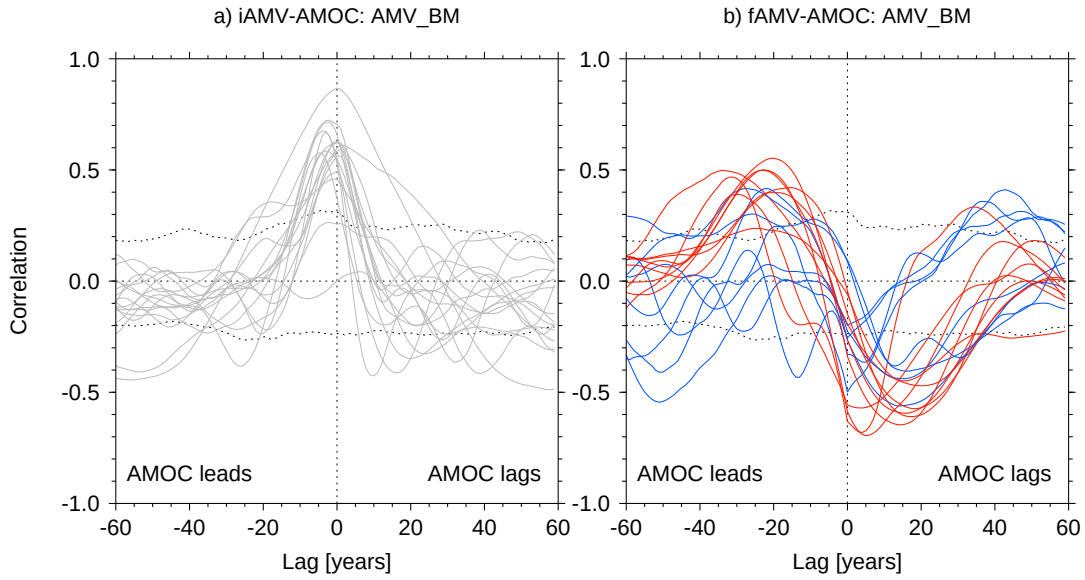

Figure S3: Shows the relationship between AMOC and internal and external components of AMV (e.g., iAMV and fAMV respectively). a) shows the cross-correlation between AMOC and iAMV-Glob for each model. Note that the correlations are based on the average of the lagged correlation computed across ensemble members of each model). Negative lags show where AMOC leads iAMV_BM, and positive lags show where AMOC lags iAMV_BM. dotted lines show the 5-95 % confidence interval based on a Monty Carlo re-sampling of AMV variability. b) shows the same, but for correlating each models ensemble-mean AMOC with fAMV-Glob for the strong (red) and weak (blue) models. Note this is the same for figure 5 in the main paper, but now for AMV_BM rather than AMV-Glob.

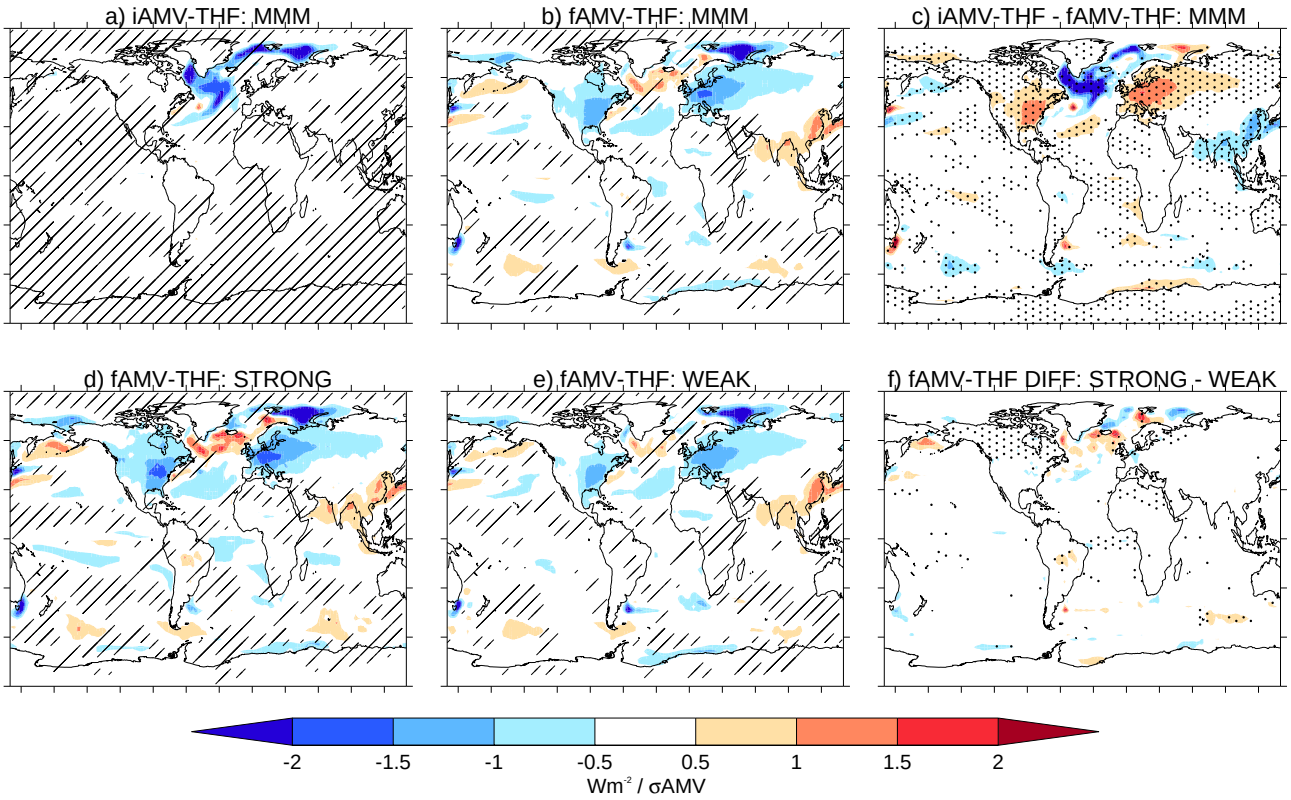

Figure S4: Shows the relationship between AMV and turbulent heat flux (AMV-THF) across internal and external components of AMV. a) the multi-model mean regression between the iAMV_BM index and turbulent heat flux at lag 0 (computed separately for each member and then averaged). Negative values shows increased turbulent heat flux out of the ocean. Hatching indicates where at least 80% of the models agree on the sign of the regression slope. b) shows the same as a) but for the fAMV_BM index. c) shows the difference, i.e., iAMV *minus* fAMV. Stippling shows where the differences in regression slopes are significantly different at the $p \leq 0.05$ level. d) and e) shows the same as b) but now for only models with strong or weak response to anthropogenic aerosols respectively (see text). f) shows the same as c) but now for the strong *minus* weak models. Note this is the same as figure 6 in the main paper, but now for AMV_BM rather than AMV-Glob.

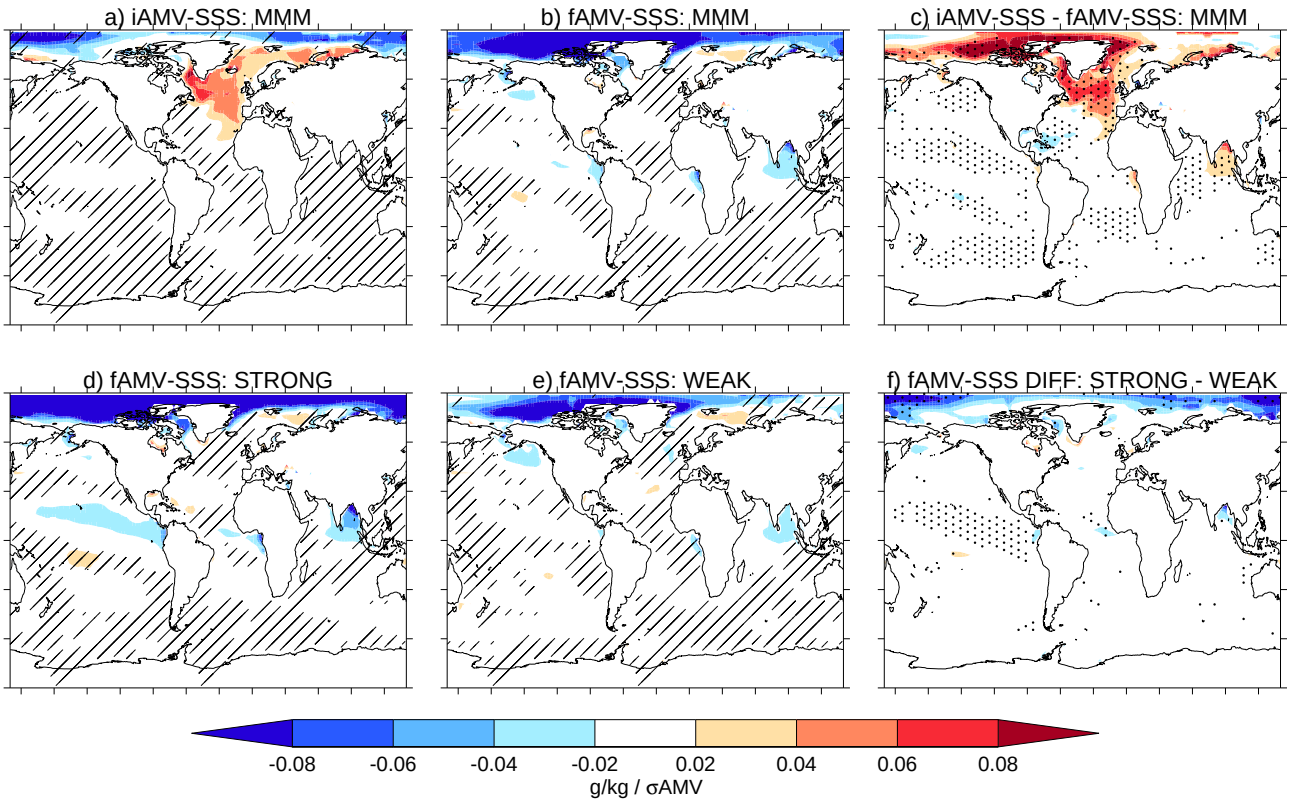

Figure S5: Shows the same as figure S4 but now for the relationship between AMV and sea surface salinity (AMV-SSS) across the internal and external components of AMV. Note this is the same as figure 7 in the main paper, but now for AMV_BM rather than AMV-Glob.

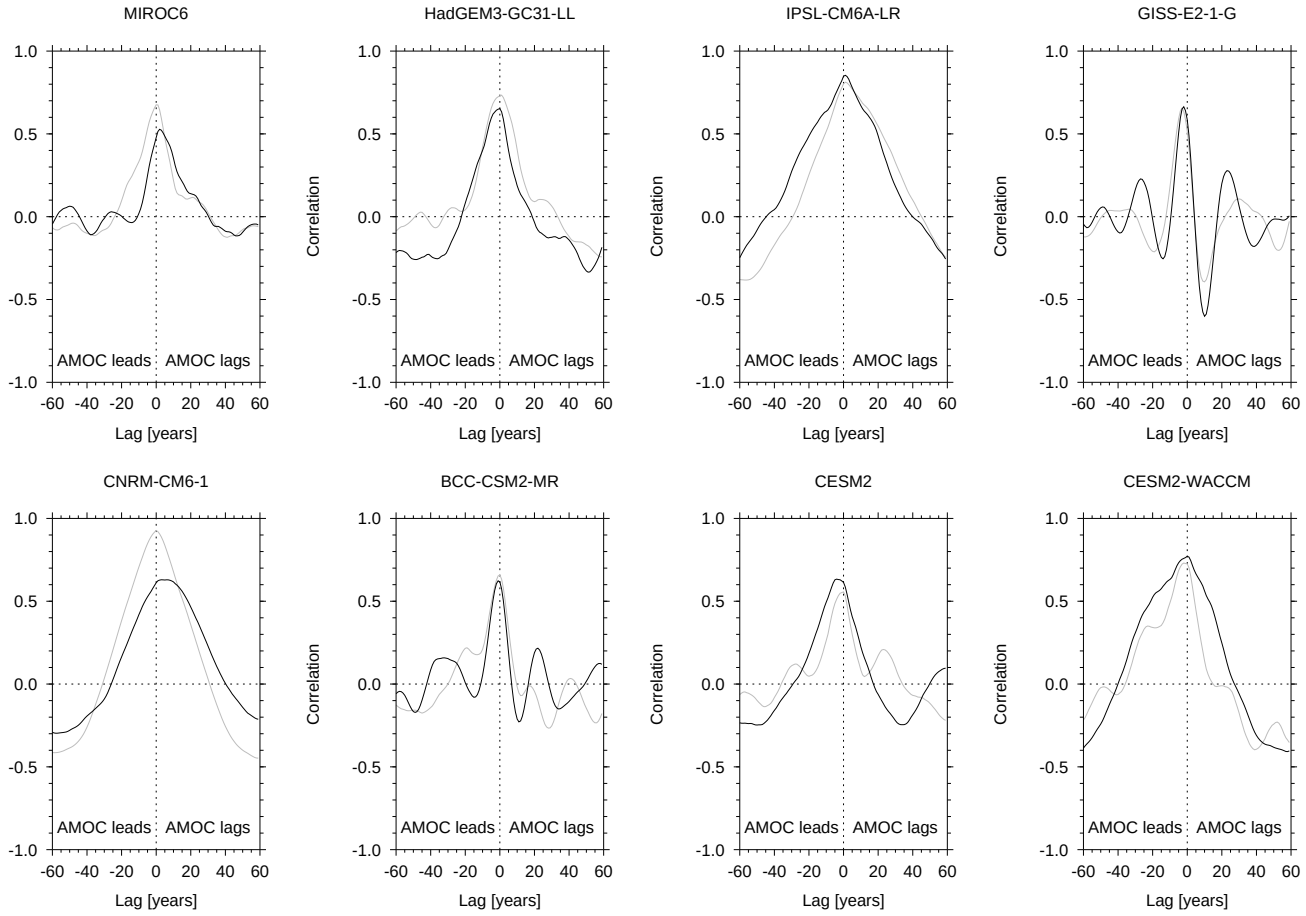

Figure S6: Shows the comparison of cross correlations between AMV and AMOC computed from the piControl (black) and using the residual method (e.g., iAMV and iAMOC, grey) for a selection of models using the AMV-Glob index. To compute the value from the control we used the first 500 years for each model, and split the time-series into overlapping chunks 165 years long to match the historical simulations. Resulting cross-correlations are averaged over all chunks. Note we do not expect the cross-correlations to be exactly the same due to sampling issues (e.g., limited members causes errors in the estimation of fAMV and fAMOC and subsequently iAMV and iAMOC), and we only use limited years. Furthermore, as shown in figure S1 the AMV-Glob does not reproduce AMV variance in models with large AMV variability and a large projection on global SSTs (in particular CNRM-CM6-1). Therefore, we expect some differences due to the method of computing AMV in the piControls.

References

Andrews, M. B., and Coauthors, 2020: Historical simulations with hadgem3-gc3.1 for cmip6. *Journal of Advances in Modeling Earth Systems*, **12 (6)**, e2019MS001 995, doi:https://doi.org/10.1029/2019MS001995, URL https://agupubs.onlinelibrary.wiley.com/doi/abs/10.1029/2019MS001995, e2019MS001995 10.1029/2019MS001995, https://agupubs.onlinelibrary.wiley.com/doi/pdf/10.1029/2019MS001995.

Boucher, O., and Coauthors, 2020: Presentation and evaluation of the ipsl-cm6a-lr climate model. *Journal of Advances in Modeling Earth Systems*, **12 (7)**, e2019MS002 010, doi:https://doi.org/10.1029/2019MS002010, URL https://agupubs.onlinelibrary.wiley.com/doi/abs/10.1029/2019MS002010, e2019MS002010 10.1029/2019MS002010, https://agupubs.onlinelibrary.wiley.com/doi/pdf/10.1029/2019MS002010.

Boucher, O., and Coauthors, 2021: Ipsl ipsl-cm6a-lr-inca model output prepared for cmip6 cmip historical. Earth System Grid Federation, URL https://doi.org/10.22033/ESGF/CMIP6.13601, doi: 10.22033/ESGF/CMIP6.13601.

Cao, J., and B. Wang, 2019: Nuist nesmv3 model output prepared for cmip6 cmip historical. Earth System Grid Federation, URL https://doi.org/10.22033/ESGF/CMIP6.8769, doi:10.22033/ESGF/CMIP6.8769.

Cao, J., and Coauthors, 2018: The nuist earth system model (nesm) version 3: description and preliminary evaluation. *Geoscientific Model Development*, **11 (7)**, 2975–2993, doi:10.5194/gmd-11-2975-2018, URL https://gmd.copernicus.org/articles/11/2975/2018/.

Danabasoglu, G., 2019a: Ncar cesm2 model output prepared for cmip6 cmip historical. Earth System Grid Federation, URL https://doi.org/10.22033/ESGF/CMIP6.7627, doi:10.22033/ESGF/CMIP6.7627.

Danabasoglu, G., 2019b: Ncar cesm2-waccm model output prepared for cmip6 cmip historical. Earth System Grid Federation, URL https://doi.org/10.22033/ESGF/CMIP6.10071, doi:10.22033/ESGF/CMIP6.10071.

Danabasoglu, G., and Coauthors, 2020: The community earth system model version 2 (cesm2). *Journal of Advances in Modeling Earth Systems*, **12 (2)**, e2019MS001 916, doi:https://doi.org/10.1029/2019MS001916, URL https://agupubs.onlinelibrary.wiley.com/doi/abs/10.1029/2019MS001916, e2019MS001916 2019MS001916, https://agupubs.onlinelibrary.wiley.com/doi/pdf/10.1029/2019MS001916.

for Space Studies (NASA/GISS), N. G. I., 2018: Nasa-giss giss-e2.1g model output prepared for cmip6 cmip historical. Earth System Grid Federation, URL https://doi.org/10.22033/ESGF/CMIP6.7128, doi: 10.22033/ESGF/CMIP6.7127.

Jungclaus, J., and Coauthors, 2019: Mpi-m mpi-esm1.2-hr model output prepared for cmip6 cmip historical. Earth System Grid Federation, URL https://doi.org/10.22033/ESGF/CMIP6.6594, doi: 10.22033/ESGF/CMIP6.6594.

Kelley, M., and Coauthors, 2020: Giss-e2.1: Configurations and climatology. *Journal of Advances in Modeling Earth Systems*, **12 (8)**, e2019MS002 025, doi:https://doi.org/10.1029/2019MS002025, URL https://agupubs.onlinelibrary.wiley.com/doi/abs/10.1029/2019MS002025, e2019MS002025 10.1029/2019MS002025, https://agupubs.onlinelibrary.wiley.com/doi/pdf/10.1029/2019MS002025.

Kuhlbrodt, T., and Coauthors, 2018: The low-resolution version of hadgem3 gc3.1: Development and evaluation for global climate. *Journal of Advances in Modeling Earth Systems*, **10 (11)**, 2865–2888, doi:https://doi.org/10.1029/2018MS001370, URL https://agupubs.onlinelibrary.wiley.com/doi/abs/10.1029/2018MS001370, https://agupubs.onlinelibrary.wiley.com/doi/pdf/10.1029/2018MS001370.

Mauritsen, T., and Coauthors, 2019: Developments in the mpi-m earth system model version 1.2 (mpi-esm1.2) and its response to increasing co2. *Journal of Advances in Modeling Earth Systems*, **11 (4)**, 998–1038, doi:https://doi.org/10.1029/2018MS001400, URL https://agupubs.onlinelibrary.wiley.com/doi/abs/10.1029/2018MS001400, https://agupubs.onlinelibrary.wiley.com/doi/pdf/10.1029/2018MS001400.

Miller, R. L., and Coauthors, 2021: Cmip6 historical simulations (1850–2014) with giss-e2.1. *Journal of Advances in Modeling Earth Systems*, **13 (1)**, e2019MS002 034, doi:https://doi.org/10.1029/2019MS002034, URL https://agupubs.onlinelibrary.wiley.com/doi/abs/10.1029/2019MS002034, e2019MS002034 10.1029/2019MS002034, https://agupubs.onlinelibrary.wiley.com/doi/pdf/10.1029/2019MS002034.

Ridley, J., M. Menary, T. Kuhlbrodt, M. Andrews, and T. Andrews, 2019a: Mohc hadgem3-gc31-ll model output prepared for cmip6 cmip historical. Earth System Grid Federation, URL https://doi.org/10.22033/ESGF/CMIP6.6109, doi:10.22033/ESGF/CMIP6.6109.

Ridley, J., M. Menary, T. Kuhlbrodt, M. Andrews, and T. Andrews, 2019b: Mohc hadgem3-gc31-mm model output prepared for cmip6 cmip historical. Earth System Grid Federation, URL https://doi.org/10.22033/ESGF/CMIP6.6112, doi:10.22033/ESGF/CMIP6.6112.

Seland, Ø., and Coauthors, 2020: Overview of the norwegian earth system model (noresm2) and key climate response of cmip6 deck, historical, and scenario simulations. *Geoscientific Model Development*, **13 (12)**, 6165–6200, doi:10.5194/gmd-13-6165-2020, URL https://gmd.copernicus.org/articles/13/6165/2020/.

Seland, y., and Coauthors, 2019: Ncc noresm2-lm model output prepared for cmip6 cmip historical. Earth System Grid Federation, URL https://doi.org/10.22033/ESGF/CMIP6.8036, doi:10.22033/ESGF/CMIP6.8036.

Sellar, A. A., and Coauthors, 2019: Ukesm1: Description and evaluation of the u.k. earth system model. *Journal of Advances in Modeling Earth Systems*, **11 (12)**, 4513–4558, doi:https://doi.org/10.1029/2019MS001739, URL https://agupubs.onlinelibrary.wiley.com/doi/abs/10.1029/2019MS001739, https://agupubs.onlinelibrary.wiley.com/doi/pdf/10.1029/2019MS001739.

Stevens, B., and Coauthors, 2013: Atmospheric component of the mpi-m earth system model: Echam6. *Journal of Advances in Modeling Earth Systems*, **5 (2)**, 146–172, doi:https://doi.org/10.1002/jame.20015, URL https://agupubs.onlinelibrary.wiley.com/doi/abs/10.1002/jame.20015, https://agupubs.onlinelibrary.wiley.com/doi/pdf/10.1002/jame.20015.

Tang, Y., S. Rumbold, R. Ellis, D. Kelley, J. Mulcahy, A. Sellar, J. Walton, and C. Jones, 2019: Mohc ukesm1.0-ll model output prepared for cmip6 cmip historical. Earth System Grid Federation, URL https://doi.org/10.22033/ESGF/CMIP6.6113, doi:10.22033/ESGF/CMIP6.6113.

Tatebe, H., and M. Watanabe, 2018: Miroc miroc6 model output prepared for cmip6 cmip historical. Earth System Grid Federation, URL https://doi.org/10.22033/ESGF/CMIP6.5603, doi:10.22033/ESGF/CMIP6.5603.

Tatebe, H., and Coauthors, 2019: Description and basic evaluation of simulated mean state, internal variability, and climate sensitivity in miroc6. *Geoscientific Model Development*, **12 (7)**, 2727–2765, doi:10.5194/gmd-12-2727-2019, URL https://gmd.copernicus.org/articles/12/2727/2019/.

Trenberth, K. E., and D. J. Shea, 2006: Atlantic hurricanes and natural variability in 2005. *Geophysical Research Letters*, **33 (12)**, doi:https://doi.org/10.1029/2006GL026894, URL https://agupubs.onlinelibrary.wiley.com/doi/abs/10.1029/2006GL026894, https://agupubs.onlinelibrary.wiley.com/doi/pdf/10.1029/2006GL026894.

Voldoire, A., 2018: Cmip6 simulations of the cnrm-cerfacs based on cnrm-cm6-1 model for cmip experiment historical. Earth System Grid Federation, URL https://doi.org/10.22033/ESGF/CMIP6.4066, doi:10.22033/ESGF/CMIP6.4066.

Voldoire, A., and Coauthors, 2019: Evaluation of cmip6 deck experiments with cnrm-cm6-1. *Journal of Advances in Modeling Earth Systems*, **11 (7)**, 2177–2213, doi:https://doi.org/10.1029/2019MS001683, URL https://agupubs.onlinelibrary.wiley.com/doi/abs/10.1029/2019MS001683, https://agupubs.onlinelibrary.wiley.com/doi/pdf/10.1029/2019MS001683.

Volodin, E., and Coauthors, 2019: Inm inm-cm5-0 model output prepared for cmip6 cmip historical. Earth System Grid Federation, URL https://doi.org/10.22033/ESGF/CMIP6.5070, doi:10.22033/ESGF/CMIP6.5070.

Volodin, E. M., and S. V. Kostrykin, 2016: The aerosol module in the inm ras climate model. *Russian Meteorology and Hydrology*, **41 (8)**, 519–528, doi:10.3103/S106837391608001X, URL https://doi.org/10.3103/S106837391608001X.

Volodin, E. M., and Coauthors, 2017: Simulation of the present-day climate with the climate model inmcm5. *Climate Dynamics*, **49 (11)**, 3715–3734, doi:10.1007/s00382-017-3539-7, URL https://doi.org/10.1007/s00382-017-3539-7.

Wieners, K.-H., and Coauthors, 2019: Mpi-m mpi-esm1.2-lr model output prepared for cmip6 cmip historical. Earth System Grid Federation, URL https://doi.org/10.22033/ESGF/CMIP6.6595, doi:10.22033/ESGF/CMIP6.6595.

Wu, T., and Coauthors, 2018: Bcc bcc-csm2mr model output prepared for cmip6 cmip historical. Earth System Grid Federation, URL https://doi.org/10.22033/ESGF/CMIP6.2948, doi:10.22033/ESGF/CMIP6.2948.

Wu, T., and Coauthors, 2019: The beijing climate center climate system model (bcc-csm): the main progress from cmip5 to cmip6. *Geoscientific Model Development*, **12 (4)**, 1573–1600, doi:10.5194/gmd-12-1573-2019, URL https://gmd.copernicus.org/articles/12/1573/2019/.

YUKIMOTO, S., and Coauthors, 2019: The meteorological research institute earth system model version 2.0, mri-esm2.0: Description and basic evaluation of the physical component. *ournal of the Meteorological Society of Japan. Ser. II*.

Yukimoto, S., and Coauthors, 2019: Mri mri-esm2.0 model output prepared for cmip6 cmip historical. Earth System Grid Federation, URL https://doi.org/10.22033/ESGF/CMIP6.6842, doi:10.22033/ESGF/CMIP6.6842.

Ziehn, T., and Coauthors, 2019: Csiro access-esm1.5 model output prepared for cmip6 cmip historical. Earth System Grid Federation, URL https://doi.org/10.22033/ESGF/CMIP6.4272, doi:10.22033/ESGF/CMIP6.4272.

Ziehn, T., and Coauthors, 2020: The australian earth system model: Access-esm1.5. *Journal of Southern Hemisphere Earth Systems Science*, **70 (1)**, 193–214, URL https://doi.org/10.1071/ES19035.